Engineering and Technology Journal e-ISSN: 2456-3358

Volume 11 Issue 06 June-2026, Page No.- 10346-10359

DOI: 10.47191/etj/v11i06.10, I.F. – 8.595

An IoT-Based Experimental Framework for Disturbance-Aware Analysis of MPPT Dynamics in Photovoltaic Systems

Ali Adnan Wahbi[1*], Kazim Majeed Murshid[2]

[1,2] Electronic and Control Engineering Techniques Department, Technical Engineering College – Kirkuk, Northern Technical University, Mosul 41001, Iraq

ABSTRACT: Under varying load, temperature and irradiance conditions, PV systems should be able to adapt to the nonlinear behavior and function with maximum power point tracking (MPPT). In most current works on MPPT, the efficiency in the steady state is the main concern, or a simulation approach is used to validate the results, few studies have explored the dynamic behavior and disturbance sensitivity under real operating conditions. A low-cost stand-alone embedded Internet of Things (IoT) based PV system is developed to test the performance of MPPT in a disturbance environment and an experimental framework is presented. The study does not propose a new MPPT algorithm, but looks at the MPPT system level performance of a standard perturb and observe (P&O) MPPT method running on a NodeMCU ESP8266 platform with integrated real-time control, DC–DC conversion, sensing, and IoT monitoring. The dynamic performance metrics are determined from the experimental data using MATLAB. The results indicate that a 40% reduction of irradiance will result in 21% increase in tracking time and steady state ripple will increase by 17 % while variations in temperature between 25 °C to 45 °C will result in less than 13 % change in tracking time. The convergence time is less than 20%, for 50% load variation, and the robustness is good. Further, a smaller perturbation step size will reduce the convergence time by up to 54%, with nearly a doubling in steady-state ripple, meaning there is a definite tradeoff between these. The study connects the dots between idealized MPPT analysis and actual PV system behavior in embedded systems when subject to disturbances in practice.

KEYWORDS: Maximum power point tracking (MPPT), Photovoltaic systems, MPPT dynamics, Disturbance-aware analysis, Embedded control, Internet of Things (IoT), Stand-alone PV systems.

1. INTRODUCTION

The energy demand for clean and sustainable energy has been growing worldwide, and PV system has been acknowledged as one of the important technologies in the modern power generation [1]. Due to their scalability, modularity and low cost, PV systems are being widely adopted in standalone PV systems, smart grid and distributed energy system [2]. The PV module characteristic is, however, nonlinear and strongly sensitive to environmental factors (including solar irradiance and temperature) [3]. This results in the operating point being continually changed, and it is necessary to use maximum power point tracking techniques in order to harvest maximum energy [4, 5].

Although decades of research have been carried out, reliable MPPT in real systems is still difficult [6]. Simple and low computational algorithms like Perturb and Observe and Incremental Conductance [7] have trade-offs between steady state oscillations and convergence rates, and they are not very successful in the presence of rapidly changing irradiances, temperatures and loads [8, 9]. The theoretical/practical performance gap is not adequately discussed in the literature. Over these setbacks, so-called intelligent and hybrid techniques have been suggested, like fuzzy logic, metaheuristic optimization and adaptive learning approaches [10]. Most studies, however, are conducted under steady-state or peak performance conditions for specific simulation and/or experimental conditions, which limits the understanding of system level dynamic behaviour and disturbance resilience.

In the meantime, technologies related with the Internet of Things (IoT) have allowed for the development of an innovative monitoring, diagnostics and supervision of PV systems by the use of real-time visualisation and long-term data logging [11, 12]. In most of the cases, however, IoT is considered to be a secondary application and not linked to the MPPT control and performance evaluation, between monitoring and control [13].

In view of these problems, this paper proposes a new approach for algorithm-independent and experimental performance evaluation of MPPT is introduced. The response curves and the dynamic performance indicators are obtained from the experimental data post-processed in MATLAB using a low cost NodeMCU ESP8266 platform. The study explores the impact of environment variations, controller parameters, sensor properties, converter dynamics and load perturbations on the MPPT performance in a single architecture instead of proposing a new MPPT algorithm.

The major contribution is a framework for the MPPT evaluation incorporating embedded control, DC–DC conversion, sensing and IoT monitoring [14]. This paper delivers an experimental investigation of the dynamic performance metrics including tracking time, steady-state ripple and recovery behavior under more realistic conditions, which takes into account disturbances unlike many earlier steady-state analyses. It also systematically allows for the quantification of the trade-off between convergence speed and steady state ripple, which facilitates practical controller tuning [15, 16]. The IoT monitoring system runs in parallel with the control loop without any influence on the execution of the MPPT. The IoT monitoring system is not dependent on the control loop and can be monitored in real-time while the MPPT is being executed. Moreover, the framework provides a link between simulation studies and actual embedded PV implementation.

The study employs the classical Perturb and Observe algorithm for clarity and reproducibility, but the evaluation framework proposed is algorithm independent and can be applied to other intelligent or hybrid MPPT algorithms for comparative evaluation.

The related MPPT literature is reviewed and gaps in the literature are identified in Section 2. The system architecture, mathematical model, embedded controller and experimental setup are presented in section 3. The results of the experiments conducted under different operating conditions are discussed in Section 4 and 5, respectively. The paper ends with Section 6 which provides a brief look at future work.

2. RELATED WORKS

In the new era of research on maximum power point tracking (MPPT), the traditional and conventional methods have been replaced by intelligent, hybrid, and system-aware approaches due to the inherent nonlinear and time-varying characteristics of photovoltaic (PV) systems. The first research projects in the early 2023s were studies on how to improve classical algorithms with a layer of adaptation that eliminate the oscillations in the steady state and allow faster convergence.

Ullah et al. [17] presented a fuzzy logic MPPT for perturb and observe (P&O) method which dynamically controls the duty cycle of the DC–DC boost converter. The method was local tracking, but was not tested under partial shading, and only showed improvement in simulation. Likewise, in [18] a metaheuristic method with salp swarm algorithm to optimize the fractional-order PID controller was proposed, which resulted in less fluctuations and faster settling time. Due to its high computational complexity, however, there are concerns about real-time implementation on low cost embedded systems.

Later, experimental attempts were made. Particularly, Del Río et al. [19] used particle swarm optimization (PSO) to control MPPT using commercial PV hardware and found that the transient response is better than that of P&O. However, the study has been limited in practice for only under constant irradiance and does not take into account the variations in load or temperature and does not account for partial shading.

PV systems with IoT came into the fore in 2024. To achieve real-time remote monitoring, Nivedha and Titus [20] proposed an IoT based monitoring framework which comprises of a high gain DC–DC converter and improved MPPT scheme. Evaluations of the performance, however, were limited and did not provide comparisons for dynamic environmental conditions. Optimisation based controllers were also investigated. Ibrahim et al. [21] introduced a nonlinear PID controller designed by genetic algorithm and PSO which was tested by simulation and HIL testing. Although the tracking has improved and the ripple has been minimized, the system was limited to a single PV–DC motor system without grid analysis. Similarly, Boussafa et al. [22] proposed a multi-stage MPPT scheme consisting of GA based voltage estimation and backstepping control the scheme has been tested and used for stable operation but the authors didn't compare it to adaptive or learning based methods and didn't tune the gains online.

Recent works of 2025 have been dedicated to grid-connected and hybrid systems. Elsafi et al. [23] analyzed the performance of the P&O and incremental conductance algorithms for a large-scale grid connected PV system but in a simulation without implementing intelligent MPPT techniques. A hybridity P&O–fuzzy–PSO method was introduced by Karimi et al. [4] and tested at a small scale, which demonstrated the superior global tracking capabilities; however, the problem of scalability, grid synchronization and voltage stability were not discussed. Adaptive learning strategies have been explored too. Turkay and Yuksek [24] presented an ANFIS-based MPPT controller that was proposed to have good convergence and lower oscillations, but no hardware validation and too much training data are needed. Placing the PID control for global MPPT in a different form [25] showed better results under partial shading, but only tested under specific shading patterns and didn't compare with adaptive approaches.

Lastly, in the literature, the transformation from classical to intelligent and hybrid MPPT techniques is seen. Most of the studies are however simulation based or have only small experimental evaluations and do not account for embedded implementation constraints, the effect of the sensors, the dynamics of the converter or the effect of real disturbance conditions. The integration of IoT is generally applied only to monitoring and not in an evaluation context of control.

This work doesn't offer a new MPPT algorithm, however. Instead, it provides a comprehensive experimental platform for the assessment of the MPPT performance under environmental changes, controller tuning, sensor and converter dynamics and load faults by implementing a low cost embedded platform based on IoT. The dynamics performance metrics are extracted from experimental data offline using MATLAB. This integrated lab-to-system approach directly confronts identified gaps and inspires the comparative analysis found in Table 1.

Table 1. Comparative Summary of Related Works on MPPT Approaches and Validation Scope

Ref.	MPPT Strategy	Validation Scope	Test Conditions	Reported Performance Metrics*	Key Observations
[17]	Fuzzy–P&O (Hybrid)	Simulation (MATLAB)	Variable irradiance and temperature	Efficiency ≈ 97%	Improved steady-state behavior over classical P&O; results limited to simulation only.
[18]	SSA-FOPID (Metaheuristic-Optimized)	Simulation (MATLAB)	Grid-connected PV–FC system	Reduced oscillation and faster settling (qualitative)	High computational complexity; no hardware or real-time validation.
[19]	PSO-based MPPT	Experimental (Real-time PV system)	Constant irradiance	Transient energy loss reduced from 31.96% (P&O) to 9.72% (PSO)	Strong experimental validation; limited disturbance scenarios.
[20]	GWO-ANN (IoT-based MPPT)	Simulation / Framework	Smart-grid PV system	Efficiency improvement reported (qualitative)	Emphasis on IoT monitoring; MPPT dynamic metrics not explicitly quantified.

[21]	GA-PSO-NPID (Hybrid Metaheuristic)	Simulation + HIL	Stand-alone PV system	Avg. efficiency ≈ 99.46%; tracking time ≈ 0.052 s	High performance under simulation/HIL; embedded complexity remains high.
[22]	GA-Backstepping Control (GA-BSC)	Experimental	Variable irradiance	Tracking time: 0.2 sec (GA-BSC) vs 0.6 sec (P&O-BSC)	Effective GA tuning; relies on offline optimization.
[23]	P&O vs Incremental Conductance	Simulation (Large-scale grid model)	Irradiance 250–1000 W/m², T = 25–50 °C	Efficiency: 98.7% (I&C), 95.2% (P&O); response time ≈ 0.15 sec	Utility-scale perspective; simulation-only evaluation.
[4]	P&O-Fuzzy-PSO (Hybrid GMPPT)	Simulation + Experimental	Partial shading	Improved global tracking (qualitative)	Tested on low-power modules; scalability not addressed.
[24]	ANFIS-based MPPT	Simulation (MATLAB)	Variable irradiance, temperature, load	Reduced oscillations vs INC (qualitative)	Adaptive behavior; no hardware validation.
[25]	PID-based Search Algorithm (PSA)	Simulation + HIL	Partial and complex shading	Faster convergence and higher GMPP tracking vs PSO/JAYA (quantitative trends)	HIL-validated; real-time embedded deployment not demonstrated.

3. METHODOLOGY

This chapter outlines the research approach used in the construction, testing, and testing of the proposed stand-alone photovoltaic maximum power point tracking (MPPT) system as part of a single experimental/monitoring system. The methodology includes the general system design, the mathematical modelling of the PV source, the dynamics of the DC-DC converter, the sensing and signal-conditioning steps, embedded MPPT control implementation and implementation of the IoT communication/monitoring. Moreover, the test protocol, performance evaluation measurements and experimental setup are all defined in systematic manner so as to establish repeatability and consistency in the assessment in varying operating conditions. The order of structuring the methodology, developing a system-level architecture to the implementation of the controllers and experimental validation, allows the creation of a clear connexion between the conceptual framework and the practical findings.

3.1. Overall System Architecture and Operating Principle

The PV power conversion system must coordinate power flow with continuous monitoring to ensure efficient operation under varying solar irradiance, temperature, and load conditions. To achieve this, an effective maximum power point tracking (MPPT) strategy is required, along with a system architecture capable of real-time sensing, embedded control, and performance monitoring. Figure 1 shows the general structure of the proposed stand-alone PV power conversion system, which integrates environmental inputs, a PV module, a DC–DC power converter, sensing and signal-conditioning circuits, a NodeMCU-based embedded controller, and an IoT cloud monitoring platform. The PV module converts solar energy into electrical energy, while the DC–DC converter regulates the operating voltage through duty-cycle control generated by the MPPT algorithm. Voltage and current sensors provide real-time feedback to the controller, enabling continuous adjustment of the operating point to track the maximum power point. Simultaneously, key system parameters are transmitted wirelessly to the cloud for remote visualization and analysis, enabling system supervision without affecting real-time control operation.

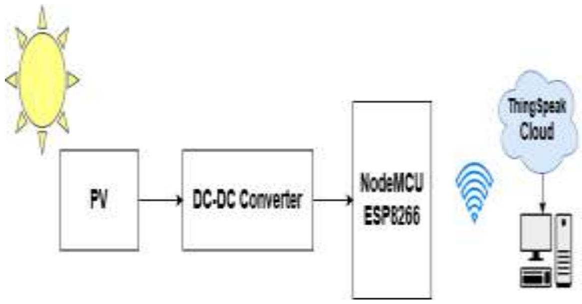

Figure 1. Overall system architecture of the proposed IoT-enabled stand-alone PV system.

The ambient temperature (T) and the amount of solar irradiance (G) directly affect the electrical properties of the PV module. The PV panel provides DC converter to DC converter which is connected to a battery or an autonomous DC load. The converter duty cycle (D) is used to adjust the operating point of the PV in real-time by a maximum-power-point-tracking (MPPT) algorithm that runs on an embedded controller. Real-time feedback to the controller is provided by voltage and current sensors, whereas the operating data are sent wirelessly to a cloud platform where they can be monitored and analysed.

3.2. Mathematical Modelling of the PV Source with Parameter Sensitivity

The photovoltaic module is simply modelled as the well-known single-diode equivalent circuit so as to enable an in-depth study of the dynamics of maximum power point tracking in various environmental factors. This model provides a realistic trade-off between analytical tractability and the necessary accuracy of assessing the MPPT performance in particular to changes in solar irradiance and temperature [26]. In the context of single-diode model, the current out of the photovoltaic module is given in Equation (1).

$$I = I_{\mathrm{ph}} - I_{\mathrm{s}}\left[\exp\left(\frac{V + IR_{\mathrm{s}}}{nV_{\mathrm{t}}}\right) - 1\right] - \frac{V + IR_{\mathrm{s}}}{R_{\mathrm{sh}}} \qquad (1)$$

Where I_{ph} is the photo-generated current, I_{s} is the diode reverse saturation current, R_{s} and R_{sh} are the series and shunt resistances, respectively, n is the diode ideality factor, and V_t is the thermal voltage defined as Equation (2).

$$V_t = \frac{kT}{q} \tag{2}$$

Where, k denoting the Boltzmann constant, T the absolute cell temperature, and q the electron charge. The above nonlinear relationship underscores the need to have a continuous maximum power point tracking (MPPT), since optimum operating voltage cannot be explicitly known and vary due to varying environment conditions. The influence of solar irradiance and temperature on electrical properties of photovoltaic devices are described in figure 2 by drawing parallel current voltage (I-V) and power voltage (P-V) curves. An increase in irradiance primarily breeds a comparable-linear increase in photo-generated current (I_{ph}), thus resulting in a significant increase in maximum recoverable power, but the voltage at the maximum power point (MPP) also changes relatively insignificantly. Contrary to this, a rise in temperature reduces the open-circuit voltage as exponential dependence on the temperature of the diode current; this effect reduces not only the potential maximum power, but also biases the MPP to lower voltage values. The observations of the associated results above imply that the MPP is always going to cross the P-V characteristic curve depending on environmental changes. In this regard, attainment of a fixed operating point leads to poor energy acquisition particularly in dynamic operating conditions. This strong sensitivity of PV characteristics to irradiance and temperature variations directly motivates the use of real-time MPPT algorithms, as implemented in the proposed system, to ensure continuous operation at or near the maximum power point.

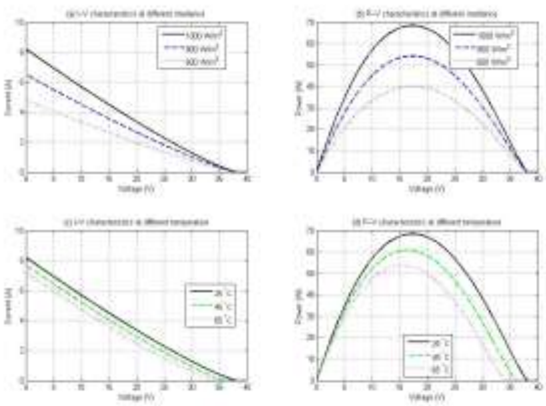

Figure 2. Influence of irradiance and temperature on photovoltaic I–V and P–V characteristics

3.3. DC-DC Converter Modelling and Dynamic Effects

The DC-DC power converter represents the main power-conditioning stage of the proposed stand-alone photovoltaic system and forms the only direct power interface between the PV panel and the load, as illustrated in Figure 3. In the adopted architecture, electrical power flows exclusively through the DC-DC converter, while voltage and current sensing circuits operate outside the power path and provide feedback signals to the embedded controller. The converter itself does not compute or generate the duty cycle; instead, it responds solely to the gate-level PWM signal produced by the microcontroller-based MPPT controller.

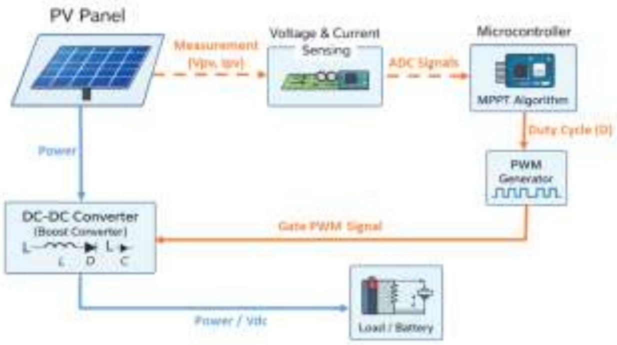

Figure 3. DC-DC converter topology and control interface used for MPPT.

The operating principle of MPPT in this system relies on indirect regulation of the PV operating voltage through duty-cycle control of the DC-DC converter. Under steady-state conditions, the voltage conversion behavior of a DC-DC converter is governed by the duty cycle D [27]. For a boost converter, which is employed in the proposed system, the voltage conversion ratio is described by Equation (3):

$$V_o = \frac{V_{pv}}{1-D} \tag{3}$$

Equation (3) indicates that changes in the duty cycle change the operating voltage of the photovoltaic (PV) system directly. As a result, any modification of the duty cycle produced by the maximum power point tracking (MPPT) algorithm causes an offset between the PV operating point on its nonlinear power voltage characteristic. The MPPT controller can optimise the PV module to the maximum power point by continually varying the duty cycle to suit changes in the environmental and load conditions. Although the derivations of Equation (3) describe the steady-state nature, the transience nature of the MPPT system is dominated by the dynamism nature of the DC-DC converter. The energy-storage components define mostly these dynamics, which are the inductor and the output capacitor. As the MPPT controller perturbs the duty cycle, energy is temporarily stored and then discharged by these components before reaching a new steady USA mode of operation.

In general, the DC-to-DC converter is not a passive power interface. Its steady-state behaviour and dynamic response is closely interconnected with MPPT behaviour. Parameters of converters directly determine speed of tracking, steady-state oscillations and resilience to environmental and loading perturbations. This high interplay between converter dynamics and MPPT behaviour inspires the parameter-effect analysis in Section 4 of this paper whereby the parameter effect of the changes in the duty cycle, transient response and ripple behaviour is quantitatively expressed in terms of experimentally measured results.

3.4. Sensing and Signal Conditioning

Proper detection of Photovoltaic voltage and current is also a primary requirement to achieve reliable maximum power point tracking as the maximum power point tracking algorithm relies explicitly on real time power estimation. Under real life conditions in stand-alone photovoltaic systems, inappropriate scaling of the signals or saturation of the sensor or noise may cause incorrect MPPT to be made or increased steady-state oscillations or reduced tracking performance. As a result, the sensing and signal-conditioning stage is carefully designed to perform measurement accuracy as well as the safe usage of embedded controller. A hybrid sensing architecture is used in this work as shown in Figure 4. The photovoltaic current is measured with a high-side current sensor, and photovoltaic voltage is measured through a resistive divider the output of which is scaled to the input count of the NodeMCU ESP8266 analog-to-digital converter (ADC). This system provides an appropriate level of compatibility with photovoltaic voltage levels used in the experimental and provides electrical isolation between the high and low power sub systems.

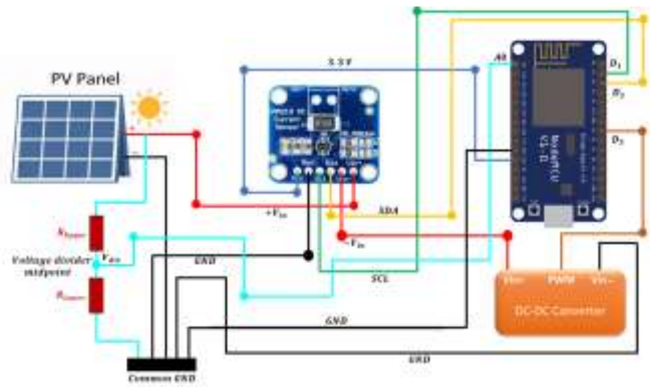

Figure 4. Voltage and current sensing and conditioning block diagram.

Figure 4 demonstrates a sensing and conditioning architecture, however; Table 2 demonstrates the electrical interconnections between the photovoltaic module, the INA219 current sensor, the NodeMCU ESP8266, the voltage-divider network, and the DC -DC converter. The table provides an accurate mapping of the power, sensing and control signals thus delivering clarity making it easy to reproducibly reproduce the experimental arrangement.

Table 2. Electrical connections for the proposed sensing and control circuit

Wire No.	From	To
1	PV panel positive (+)	INA219 VIN+ (high-side current sensing input)
2	PV panel negative (−)	Common ground
3	INA219 VIN− (high-side current sensing output)	DC–DC converter input positive (+)
4	DC–DC converter input negative (GND)	Common ground
5	NodeMCU ESP8266 3.3 V	INA219 VCC (3.3 V logic supply)
6	INA219 GND (logic ground)	Common ground
7	INA219 SDA	NodeMCU D2 (GPIO4)
8	INA219 SCL	NodeMCU D1 (GPIO5)
9	PV panel positive (+)	Upper resistor of voltage divider (R_{upper})
10	Voltage divider midpoint (V_{div})	NodeMCU A0 (ADC)
11	Lower resistor of voltage divider (R_{lower})	Common ground
12	NodeMCU ESP8266 PWM output	DC–DC converter PWM control or gate-driver input

3.5. Embedded MPPT Control Using NodeMCU ESP8266

The proposed stand-alone photovoltaic system uses the NodeMCU ESP8266 as the core embedded controller of the system, which combines the MPPT control, real-time sensing, and communication into one low-cost platform. In every control cycle, the controller receives the conditioned photovoltaic voltage V_{pv} and photovoltaic current I_{pv} signal, calculates the instantaneous PV power and runs the MPPT algorithm to get the corresponding adjustment of the duty-cycle. The MPPT algorithm produces a command D that is a duty-cycle that is the required ratio between the ON and the switching period of the PWM signal on the DC-DC converter. This duty cycle command is an official control element that is varied at every sampling moment on the footing of the MPPT choice rationale. The PWM charge of the NodeMCU converts the duty-cycle command D to a tangible pulse-width modulated signal which directly influences the switch-behavior of the DC-DC converter and determines the operating-point of the photovoltaic module. The resultant duty cycle is produced as a pulse-width modulated (PWM) signal and fed to the switching element of the DC-DC converter, thus controlling the PV operating voltage as well as imposing significant operation close to the maximum power point as in Figure 5.

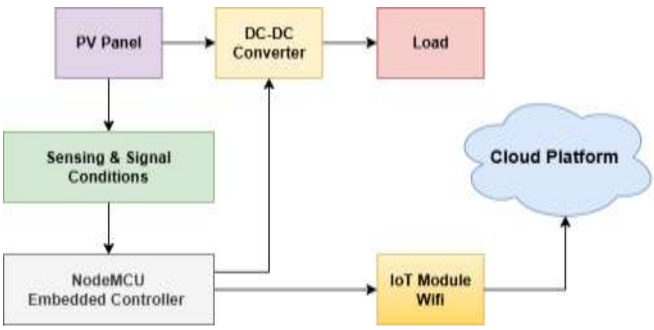

Figure 5. Functional block diagram of the NodeMCU-based MPPT control loop.

This design of closed-loop control is used to enable constant monitoring of the maximum power point regardless of the changes in solar irradiance, temperature, and isolated load conditions. In this paper, a perturb and observe based maximum power point tracking (MPPT) is used because of its simplicity and simple computation requirements and because of its ability to operate well as a device on resource-limited embedded hardware. To base the presentation of the MPPT algorithm on an analytical form, and demonstrating it in $Algorithm$ 1, the analysis-independent information is provided, whereas no implementation-related issues are included. The algorithm functions by, as far as the converter duty-cycle is concerned, making infinitesimal adjustments to the converter duty-cycle and measuring the resultant change in photovoltaic power to determine the direction towards the maximum power point [28]. Furthermore, compared with the previously stored value $P(k-1)$. The corresponding power variation is defined as Equation (4).

$$\Delta P = P(k) - P(k-1) \tag{4}$$

Based on the sign of ΔP, the controller determines whether the most recent duty-cycle perturbation improved or degraded the operating point. If $\Delta P > 0$, the perturbation direction is retained; otherwise, it is reversed. Accordingly, the duty cycle is updated as Equation (5).

$$D(k) = D(k-1) \pm \Delta D \tag{5}$$

Where ΔD denotes the perturbation step size. These expressions are provided to formally describe the implemented control logic rather than for direct analytical performance prediction. The updated duty cycle is subsequently applied to the DC-DC converter through the PWM output of the NodeMCU. The step-by-step execution of the embedded MPPT algorithm implemented on the NodeMCU ESP8266 is formally described in $Algorithm$ 1.

Algorithm 1. Perturb and Observe (P&O) MPPT logic for boost converter

“Measure the photovoltaic voltage $V_{pv}(k)$ and current $I_{pv}(k)$.”
“Compute the instantaneous power $P(k) = V_{pv}(k)I_{pv}(k)$.”
“Evaluate the power and voltage variations $\Delta P = P(k) - P(k-1)$ and $\Delta V = V_{pv}(k) - V_{pv}(k-1)$.”
“For a boost converter, update the duty cycle according to the following rules:
If $\Delta P > 0$ and $\Delta V > 0$, decrease the duty cycle.
If $\Delta P > 0$ and $\Delta V < 0$, increase the duty cycle.
If $\Delta P < 0$ and $\Delta V > 0$, increase the duty cycle.
If $\Delta P < 0$ and $\Delta V < 0$, decrease the duty cycle.”
“Update $P(k-1) = P(k)$, $V_{pv}(k-1) = V_{pv}(k)$, and apply the updated duty cycle.”

The embedded MPPT routine is outlined in the presented $Algorithm$ 1. To determine the change of power, conditioned photovoltaic voltage and current measurements are used to calculate instantaneous power and the comparison is then made with the previous value. This difference, along with the perturbation of the voltage, defines whether the direction of perturbation of the duty-cycle is maintained or reversed in connection with classical P&O rules. The renewed duty cycle is fed to the DC - DC converter through the PWM, and the duty cycle restarts, thus allowing the continuous maximum power point tracking. Elementary arithmetic and conditional branching are used to instantiate the algorithm, which has been proven to work well on the limited computational resources of the ESP8266 microcontroller. The tuning parameters of the dynamic performance depend on the perturbation step size ΔD and update interval in particular. The bigger the perturbation step or faster the update, the greater the transient response however; the greater the steady state oscillation; and vice versa. This is an experimental measure of this trade-off in Section 4.

3.6. Controller Implementation Details (NodeMCU ESP8266)

The controller is designed within the computational and timing limits of the NodeMCU ESP8266 to maintain deterministic MPPT operation. A fixed-rate loop handles signal acquisition, MPPT calculation, and duty-cycle update, while lower priority tasks handle monitoring and communication. At period Ts, PV voltage and current are sampled to define MPPT execution. Power is calculated at each step and the duty cycle is adjusted using P&O logic for consistent behavior across tests. PWM runs at a higher frequency than MPPT updates to reduce ripple. The NodeMCU generates the PWM signal for the converter, balancing switching losses, ripple, and resolution. Signals are conditioned before ADC conversion due to its narrow input range, ensuring accurate power estimation and real-time processing. Simple filters (e.g. moving average) reduce noise without adding delay that would distort dynamic response. Real-time control is separated from cloud communication. MPPT runs at a fixed rate, while data is sent at a lower rate to avoid network delays affecting stability. The architecture achieves stable real-time MPPT operation under varying conditions, showing that effective MPPT and IoT monitoring can be implemented on a low-cost embedded system without degrading performance.

3.7. IoT Communication and Cloud Monitoring

The suggested system uses an IoT as the communication layer to provide the possibility to track the photovoltaic system work round the clock and analyze the results after the work, but fully deterministic embedded MPPT control can be ensured. With the inbuilt Wi-Fi functionality of the NodeMCU ESP8266, relevant variables in the system will be intermittently sent to a cloud-based monitoring system. These variables are; photovoltaic voltage, V_{pv}, photovoltaic current, I_{pv}, output power, P_{pv} and the MPPT duty cycle D. The data transmission period is specifically made independently of the MPPT control loop to allow communication latency, packet loss or network instability to have no effect on control execution.

Figure 6 illustrates that there is a single direction of data flow in the IoT architecture, i.e., the embedded controller to the cloud platform. The whole sensing, MPPT decision-making, and duty-cycle updates are done locally in the NodeMCU, but the cloud layer has only a supervisory interface. This rigid division between monitoring and control maintains deterministic MPPT timing as well as ensures consistent operation during dynamic environmental and load conditions.

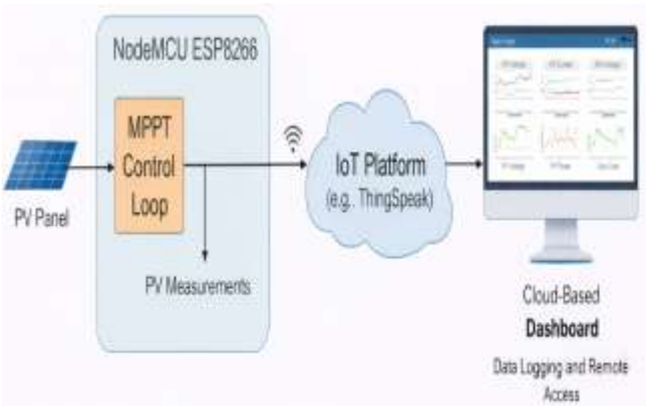

Figure 6. IoT communication framework and cloud-based monitoring dashboard.

The communication and cloud-linked surveillance layer of IoT is a non-invasive oversight device that acts as an extension of the on-board MPPT controller. Enabling real-time visualization and long-term data recording without being involved in control decisions, the proposed architecture allows conducting an entire experimental analysis of the experimental and enhances the practical significance of the offered MPPT framework.

3.8. Experimental Setup and Parameter-Effect Evaluation

This section outlines the proposed stand-alone photovoltaic maximum power point tracking (MPPT) system implementation and discusses the methodology to be used in the assessment of system parameters effect. The experimental setup, along with the identification of the hardware functionality, is not only used to confirm its functionality but also to provide a controlled, reproducible system to examine the effect of system parameters on the performance of MPPT in realistic operating conditions.

The proposed system presented in Figure 7 is the experimental version that includes a photovoltaic module, DC-DC power converter, voltage and current sensors, a NodeMCU ESP8266 embedded controller and a DC load/store stand-alone power unit. Such constituents are gathered into a closed power-conversion platform which provides real-time MPPT control and IoT connectivity. The modular structure is used to ensure safe working conditions, enable the adaptable change of parameters, and to allow the easy observation of the system dynamics during testing.

Figure 7. Experimental prototype of the proposed stand-alone PV MPPT system.

The experimental photovoltaic system was implemented using a 60 W monocrystalline PV panel operating under varying irradiance and temperature conditions. The PV module operates with a maximum power voltage in the range of 17–18 V and an open-circuit voltage of approximately 21–22 V. A 12 V stand-alone battery/load unit was connected at the converter output to emulate practical operating conditions. The system integrates a boost DC–DC converter controlled by a NodeMCU ESP8266 executing the perturb and observe (P&O) MPPT algorithm. Real-time voltage and current measurements were obtained using a resistive voltage-divider circuit and an INA219 high-side current sensor, respectively. Experimental measurements demonstrated an average MPPT efficiency of approximately 98.1% across all tested operating scenarios.

The photovoltaic module provides electrical energy to the DCDC converter via a sensing stage where voltage and current is measured and conditioned before being handled by an on board controller. According to the measurements, the NodeMCU performs the maximum power point tracking (MPPT) algorithm, locally and compares it with the pulse-width modulated (PWM) signal to control the duty cycle. The controller moves the operating point of the photovoltaic array, regardless of the changes in loads or environment, by continually changing the duty cycle to reach the maximum power point (MPP). The DC-to-DC converter couples the PV source to a standalone load thus allowing a realistic study of the MPPT dynamics. At the same time, specific system variables are sent to the cloud to monitor and log data (Section 3.7). This monitoring is purely decoupled with the control loop and plays no role in the MPPT execution. This means that the cloud layer is strictly overseeing and does not introduce any dynamics into the systems since it only helps to observe systems. The experimental system explores several aspects that influence the MPPT behavior: environmental (irradiance, temperature), converter (inductance, capacitance, switching frequency), sensing and sampling (characteristics), MPPT tuning parameters, and load (variations) as well. Both of them affect tracking speed, steady state oscillations, and energy harvest efficiency. To analyze it systematically, the ranges of parameters and scenarios are captured in Table 3. A single parameter is varied whilst the rest are held constant thus isolating the effect of each factor and allowing a reasonable comparison among test cases.

Table 3. Tested parameter ranges and experimental scenarios for MPPT performance evaluation

Category	Parameter	Symbol	Tested Values
Environmental	Solar irradiance	G	400, 600, 800, 1000 W/m^2
Environmental	PV temperature	T	(25, 35, 45) °C
MPPT Control	Perturbation step size	ΔD	0.005, 0.01, 0.02
MPPT Control	MPPT update period	T_{MPPT}	(50, 100, 200) ms
Sensing & Sampling	Sampling period	T_s	(5, 10, 20) ms
Sensing & Sampling	Digital filter window	N	(3, 5) samples
Load Conditions	Stand-alone load variation	---	Constant / step change
IoT Monitoring	Data upload interval	---	(5–30) s

Mathematically, the performance of MPPT is modelled as the ratio of the electrical energy delivered to the load and the greatest achievable photovoltaic energy in the same observation period as indicated in Equation 6 [29].

$$\eta_{\text{MPPT}} = \frac{\int_0^T P_{\text{out}}(t)\,dt}{\int_0^T P_{\max}(t)\,dt} \times 100\% \qquad (6)$$

Where $P_{\text{out}}(t)$ is the measured output power and $P_{\max}(t)$ represents the maximum achievable PV power under the corresponding environmental conditions. The definition of performance that is given next is based on experimental findings instead of on models that are derived from analysis. In addition to the efficiency, the study generates dynamic performance measures such as tracking time, steady state ripple, post-disturbance recovery behaviour, etc. of the measured power response, which are then analysed in the results section.

In order to guarantee reproducibility, all the experiments were done using a common embedded firmware, fixed MPPT logic, and strictly defined ranges of parameters. Each trial involved changing one parameter and keeping the rest constant and measurements were taken at the same period of time. All cases where homogeneous configurations could be sensed, sampled and monitored were repeated in an independent manner under similar hardware and operating conditions, which ensured the validity of the findings of the reports.

The experimental structure and the parameter-effect evolutional approachology give a strictly pure basis to the disturbance conscious MPPT analysis which goes ahead. The proposed methodology allows for the gap between the idealized investigations performed on the model of MPPT and the stand-alone operation of PV systems to be closed by coupling realistic implementation of the hardware and by varying the parameters and applying the same metrics for the operation of the PV systems.

3.9. Test Protocol for the Parameter-Effect Study

This part outlines the experimental procedure that aimed to analytically determine the effect of the contributing factors on the dynamic and steady-state of Maximum Power Point Tracking (MPPT). The protocol allows a fair comparison between, repeatability and actual attribution of change in performance to certain parameter alteration.

The result of all experimental trials was obtained using the configuration described in Section 3.8 and described in Figure 7. Before the test, the system was started with a fixed set of conditions in order to enable the MPPT algorithm to reach a point near the Maximum Power Point (MPP). A controlled disturbance was then introduced at the steady state, as suggested by the test scenario. The disturbances included environmental changes (irradiance, temperature), MPPT tuning changes, sensing and sampling changes, and load step changes. Each of the tests changed one parameter, and all the other parameters were held constant so that the effect of a particular parameter on the behavior of the MPPT could be isolated.

Dynamic metric extraction was uniformly extracted using wave-form based evaluation among test cases. Figure 8 above shows the reference response: an imposed disturbance at a fixed point causes a temporary off-point the resultant power response is then recorded resulting in a measure of tracking duration and steady-state oscillations.

In Figure 8 we show two sample responses highlighting the impact of MPPT tuning. The fast-tuned response is characterized by quick convergence and significant overshoot industry and a strong show with large perturbation steps or higher rates of update at the cost of ripple. On the other hand, the slow-tuned response has smooth gradual convergence with less overshoot and low oscillations though with a longer tracking time. These opposite cases represent the inherent trade of convergence rate and steady-state stability of perturbation-based MPPT algorithms.

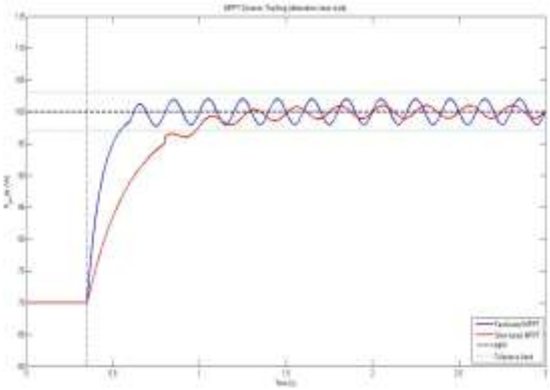

Figure 8. Reference MPPT power response for tracking time and steady-state ripple extraction

The dashed horizontal line in Figure 8 represents the maximum-power point (MPP), and we ostracize the bounds as a tolerance band that surrounds the MPP. Operationally, tracking time is defined to be the duration between the instant of disturbance through which the photovoltaic power begins and continues to exist within the same band. This definition excludes temporary peaks and momentary crossings as having been mistaken as successful convergence, so as to have an objective comparison of all test cases.

After convergence, steady-state oscillations are evaluated during the given time interval (Figure 8). The sources of these oscillations are the perturb-and-observe (P&O) perturbation mechanism, converter switching dynamics and measurement noise. The steady-state ripple is defined as the difference between the maximum and minimum power value divided by the average value as in Equation (7). This standardized measure enables equal comparisons of dissimilar operating points, irradiance levels and power scales [30].

$$\mathrm{Ripple}(\%) = \frac{P_{\max} - P_{\min}}{P_{\mathrm{avg}}} \times 100 \qquad (7)$$

Where $P_{\max}$, $P_{\min}$, and P_{avg} represent the maximum, minimum, and average photovoltaic power values measured during the steady-state interval following MPPT convergence. All test cases were carried out under constant observation period where photovoltaic voltage, photovoltaic current, output power and duty cycle were recorded continuously. The data were collected through the in-built nodeMCU controller and then manually offline through the use of MATLAB to uncover the predetermined performance measures. To maximize the level of reliability, individual experiments were repeated severally under the same conditions and the representative responses that showed consistency in the repeated experiments were used as the basis of analysis.

Combining parameter variation control with waveform-based extraction of metrics, as demonstrated in Figure 8, will give the proposed test protocol an inflexible, disturbance-conscious protocol of testing maximum power point tracking (MPPT) behavior. The protocol guarantees tracking time, steady-state ripple and recovery behavior are consistent values based on experimentally measured values, as reported in Section 4 and summarized in Table 4 and therefore are fairly compared at the various operating conditions and parameter regimes.

3.10. Definition of Experimental Test Cases

The experimental research utilizes the use of predetermined test cases (Table 3) in order to isolate the particular parameter impacts on maximum power point tracking (MPPT) performance.

1) Case C1 (Baseline): Reference steady-state performance is determined by setting case conditions to nominal ($1000\ W/m^2, 25°C$).
2) C2 and C3 (Irradiance variation): Steady-state tracking of lower power levels comprises cases with constant irradiance levels ($800, 600\ W/m^2$).
3) Cases C4-C5: (Dynamic irradiance): The transient response and recovery to step changes ($600 \rightarrow 1000, 1000 \rightarrow 600\ W/m^2$) are tested.
4) Case C6 (Temperature variation): MPPT is studied under high temperature ($45°C$) in order to observe the adaptation to changes in voltage.
5) Cases C7-C9 (Tuning parameters): Minimal, medium and large perturbation step sizes (ΔD) are explored so as to determine the trade-off between the speed of convergence and steady-state ripple.
6) Cases C10-C11 (Load robustness): It is tested with the steps of loading of the machine by $\pm 50\%$ in order to ensure the stable operation of the machine and recovery of its MPP to load disturbances.
7) Case C12 (Overall performance): Summative measures in all the scenarios are provided.

Each case is analyzed according to the procedure described in Section3.9, and metrics are extracted in the form of waveforms (Figure9). Findings have been described in Section 4 and Table 4.

4. RESULTS

The steady-state waveforms represent confined oscillations that are due to the intrinsic perturbation mechanism of the P&O algorithm, switching ripple of the DC-DC converter and measurement noise, which proves that MPPT can properly operate in a practical environment. The small scale of these vibrations shows a stable trade-off between tracking error and stability ripple. To make the explanation clearer, Table 4 presents the summaries of the most important quantitative performance indicators: tracking time, steady-state oscillation and MPPT efficiency. These steady-state, dynamic response and sensitivity of a parameter, and robustness are then demonstrated through detailed analysis of representative experimental waveforms in Figures 10-16. All the result curves and performance values are determined with experimentally measured data and then processed and plotted with MATLAB so that there is consistency of analysis and comparison.

Table 4. Quantitative MPPT performance metrics obtained for the experimental test cases

Case	Test Condition	Tracking Time (Sec)	Steady-State Ripple (%)	MPPT Efficiency (%)	Remarks
C1	Nominal conditions (G = 1000 W/m², T = 25°C)	0.62	1.8	98.9	Baseline steady-state performance
C2	Reduced irradiance (G = 800 W/m²)	0.68	1.9	98.6	Stable tracking at lower irradiance
C3	Low irradiance (G = 600 W/m²)	0.75	2.1	98.1	Slightly slower convergence
C4	Irradiance step: 600 → 1000 W/m²	0.84	2.3	97.8	Fast transient recovery
C5	Irradiance step: 1000 → 600 W/m²	0.92	2.5	97.4	Larger transient dip observed
C6	Elevated temperature (T = 45°C)	0.7	2	97.9	MPP shifts to lower voltage
C7	Small MPPT step size (ΔD = small)	1.05	1.2	99.1	High steady-state efficiency
C8	Medium MPPT step size (ΔD = nominal)	0.72	1.9	98.8	Balanced response
C9	Large MPPT step size (ΔD = large)	0.48	3.6	97.2	Fast tracking, higher oscillation
C10	Load step: +50%	0.88	2.4	97.6	Robust recovery under load increase
C11	Load step: −50%	0.81	2.2	97.8	Stable response after unloading
C12	Aggregate performance (all cases)	0.78 (avg.)	2.2 (avg.)	98.1 (avg.)	Overall system performance

4.1. Steady-State MPPT Performance under Constant Irradiance (Cases C1–C3)

The steady-state tracking output of the suggested MPPT controller is studied under constant irradiance and temperature laws of the Cases C1-C3. Based on nominal operating conditions (Case C1), the controller quickly approaches maximum power point and remains at constant operation with only slight steady-state oscillations. It is made up of this observation which forms a reference point of future comparative analyses. Figure 9 presents the steady-state response at nominal conditions where the photovoltaic operating point is strongly congregated at the maximum power point after convergence has been reached.

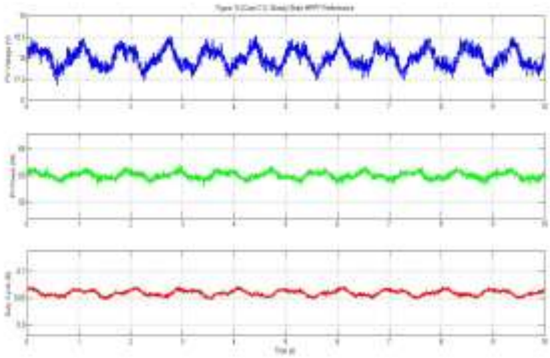

Figure 9. Steady-state MPPT performance under nominal operating conditions (Case C1).

The stable oscillations of the steady-state waveforms are assignable to binding oscillations by the perturb and observe algorithm implicit perturbation mechanism, converter switching ripple, and measurement noise, and hence it proves that the MPPT operates stably under practical conditions.

Figure 10 shows the steady-state MPPT operation at low irradiance at Case C2 and C3. The photovoltaic power approaches about 48 W at 800 W/m^2 and 36 W at 600 W/m^2, which proves the expected proportional reduction of the available power as irradiance is reduced. This means a successful convergence to the maximum-power point, which is indicated by the unavailability of long-term drift as well as little, bounded oscillations.

The reported constant ripple is limited to the fractions 1.9 and 2.1%, respectively, in Case C2 and Case C3, which is consistent with the quantitative results summarised in Table 4 and with the behaviour of perturbation-based MPPT algorithms under normal conditions. The values of ripple have been reported as the variation between peak and steady-state power (peak to peak) as per Section 3.9.

At the region near the MPP voltage the PV voltage level is constant and at the duty-cycle response converges to the constant mean values corresponding to the various irradiance levels. These findings are all indicative of consistent steady-state MPPT operating in low irradiance environments, which are typified by constant power harvesting and minimal oscillatory characteristics.

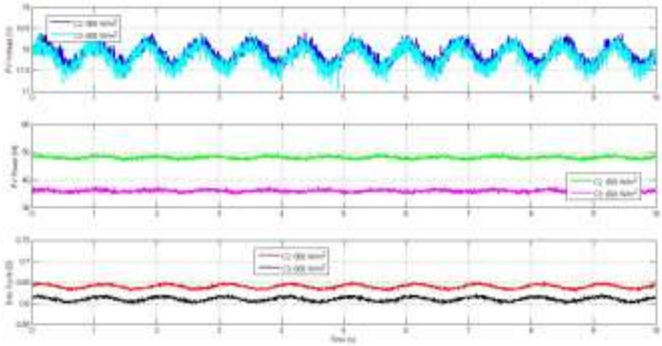

Figure 10. Steady-state MPPT performance under reduced irradiance levels (Cases C2–C3).

4.2. Dynamic MPPT Response under Irradiance Step Variations (Cases C4–C5)

The dynamic tracking operation of the proposed MPPT controller was evaluated under a rapidly increasing step of the irradiance that aimed at representing momentary cloud conditions. When the irradiance changed between 600 to 1000 W/m2 (Case C4), the operating point of the photovoltaic briefly changed to a position above the maximum power point, which caused the controller to respond by modulating the duty-cycle. It can be observed that the extracted PV power increases rapidly and stabilizes at the new steady-state operating point within a relatively short period; thenceforth, the operation around the MPP is stable with minor marginally bounded fluctuations as shown by Figure 11.

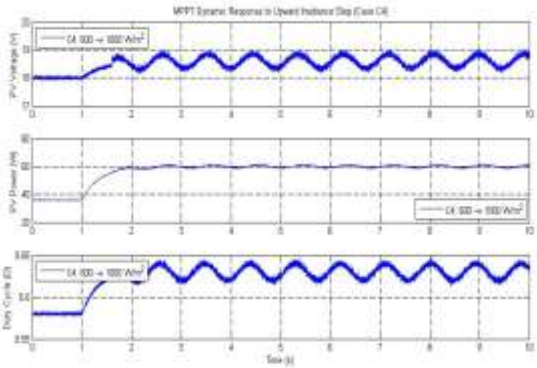

Figure 11. MPPT dynamic response to an upward irradiance step transition (Case C4).

In order to evaluate the strength of the suggested MPPT controller during sudden changes in the solar flux, a downward irradiance step is implemented to introduce a simulated event of sudden cloud-shadowing. As Figure 12 depicts, a step of irradiance of 1000 to 600 W/m^2 (Case C5) leads to severe transient decrease in power and quick recovery. The MPPT controller reaches the new operating point in about 0.92 sec and stabilizes in operation with steady-state operating power that is around 2.5% in ripple, which is in line with the performance parameters presented in Table 4. The ripple values are reported as the difference between the peak and steady-state power variation calculated by reference to the definition of the steady-state power variation of Section 3.9.

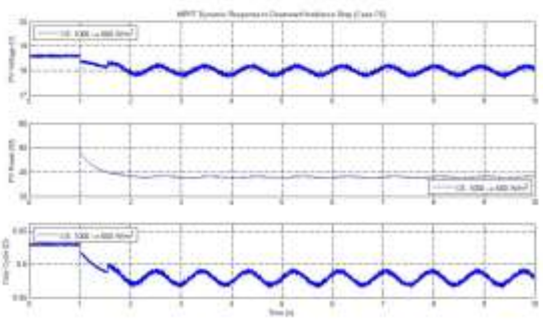

Figure 12. MPPT dynamic response to a downward irradiance step transition (Case C5).

4.3. Effect of Temperature Variation and MPPT Tuning Parameters (Cases C6–C9)

This subsection explores how variations in photovoltaic (PV) temperature affect dynamical tracking performance of photovoltaic systems as well as the influence of maximum power point tracking (MPPT) tuning on system performance. As compared to the changes in irradiance, changes in temperature mainly influence the voltage characteristics of the PV module causing the maximum power point (MPP) to shift along the voltage axis. Furthermore, the impact of the various MPPT step-size values on a convergence rate, steady-state oscillation and just the tracking efficiency is evaluated to determine the stability of the given control strategy in various operating environments.

The thermal variations affecting the performance of MPPT are investigated by heating the PV module and keeping the irradiance constant. The curve in Figure 13 indicates that the MPP moves at a lower voltage with an increase in temperature of the PV between $(25 - 45)$℃ and also, the power decreases by a small margin. The MPPT controller quickly changes, steady-state of 0.7 sec converting to the new operating point with a steady-state power ripple of approximately 2% in agreement with the quantitative findings in Table 4.

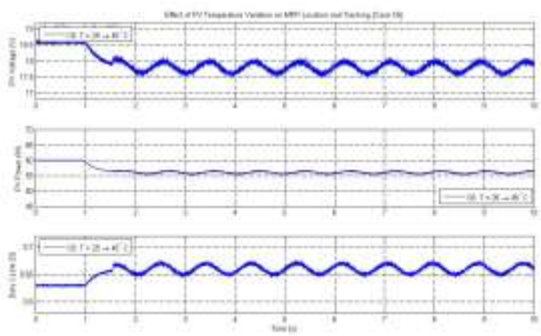

Figure 13. Effect of PV temperature variation on MPP location and tracking behavior (Case C6).

The convergence velocity and steady-state oscillations in the MPPT algorithm are directly proportional to the perturbation step size. Three different step sizes were tested to determine this influence under the same operating conditions (Cases C7 and C9). Figure 14 shows that the operation of MPPT starts at t = 1 sec. A very small perturbation step size (C7) is the slowest to converge to the steady state (around 1.05 sec) and it achieves the lowest steady-state power ripple (around 1.2%). On the other hand, a large step size (C9) provides the quickest tracking (about 0.48 sec), but with increased oscillations, so the power ripple increases to about 3.6%. The step size (C8) is a good test as the response is convergent (C8) and at the same time the ripple is moderate (1.9%). The fact that these observations indicate a trade-off between the convergence speed and steady-state ripple is a clear indication that the performance metrics compiled in Table 4 are supported.

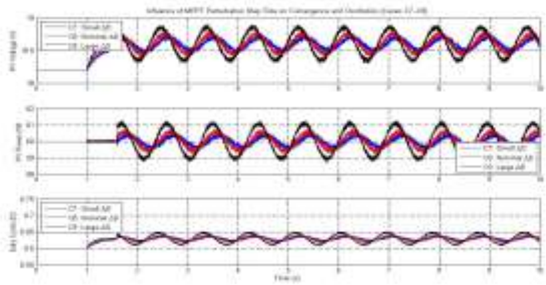

Figure 14. Influence of MPPT perturbation step size on convergence speed and steady-state oscillation (Cases C7–C9).

4.4. Robustness under Load Disturbances and Overall Performance (Cases C10–C12)

The Load variation is a common perturbation in a real world stand-alone photovoltaic system, which can have a major effect on system stability and power recovery efficiency. In order to estimate the strength of the suggested MPPT strategy in such conditions, dynamic response was considered in response to sudden changes in loads steps and under the general conditions of operation. In particular, the performance of the system under both the increase and decrease events of the load (Case C10 and C11) were tested, and, finally, the overall performance of the system across all test cases (Case C12) was determined, hence, a comprehensive figure of monitoring stability and convergence rate and steady-state behaviour.

Figure 15 shows the response of the MPPT to load disturbances of the stand-alone mode caused by a +50% load increase (Case C10) and a -50% load decrease (Case C11), at t=1 sec. The change in load in both cases leads to a temporal shift in the PV operating point as indicated by the presence of a power dip in C10 and a power overshoot in C11. In CaseC10, the MPPT controller is quick to adjust the load demand up and is able to resume operation at the peak power point within a time of about 0.88 sec with a steady-state power ripple of nearly 2.4%. In Case C11, the system is stabilised once it has been unloaded in 0.81 sec with a slightly smoother ripple of about 2.2%. These findings can indicate the ability of the offered MPPT scheme to maintain constant functionality and successful tracking in the case of sudden changes in loads, which is consistent with the performance parameters in Table 4.

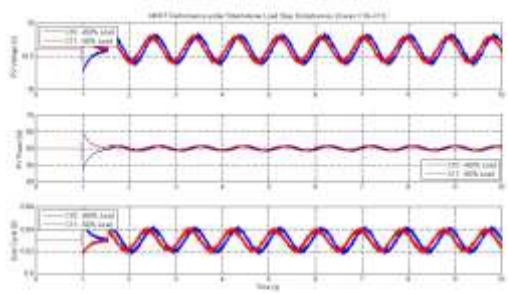

Figure 15. MPPT performance under stand-alone load step disturbances (Cases C10–C11).

To provide the full evaluation of the suggested MPPT strategy, the system overall performance is studied through the analysis of the accumulation behaviour of the controller under all of the operating regimes. The summary of the analysis is that the joint effect of tracking velocity, steady-state stability, and disturbance robustness can provide an exemplary measure of the effectiveness of MPPT under actual working conditions.

Figure 16 shows the general performance of the MPPT in the real operating conditions, thus giving a general assessment of the controller behaviour in all the cases of the tests.

After the perturbation made at t = 1 sec, the photovoltaic voltage, power and duty cell experience a short-term transient and stabilize to the new working point in a smooth manner. The MPPT controller restarts operation at the maximum power point in about 0.78 sec, which is consistent with the reported average tracking time of Table 4.

In steady state, it can be seen that the extracted power exhibits reasonable oscillations with an average ripple of around 2.2 and is indicative of stable and effective tracking. These results confirm the fact that the suggested MPPT strategy provides the most appropriate trade-off between fast convergence and low steady-state oscillation, and, therefore, it proves the good general performance of a system.

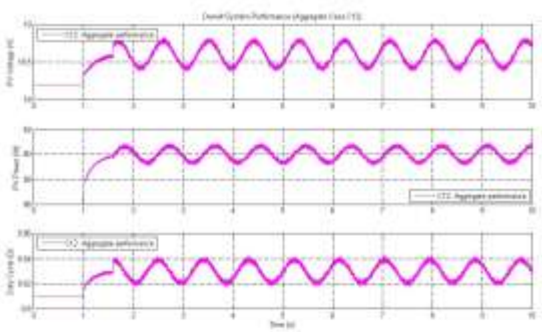

Figure 16. Overall system performance – Case C12.

5. DISCUSSION

The presented Figures 9-16 and Table 4 give a detailed description of the dynamic and steady-state operation of the proposed MPPT strategy over a range of operating conditions. Instead of only considering peak efficiency, the analysis preempts the transient behavior of the controller, which is an important factor with regard to practical PV systems.

At high rates of irradiance fluctuations (Cases C4-C5) the MPPT controller is shown to converge very quickly to the newly determined MPP when irradiance changes abruptly. Whereas temporary deviations of optimum operating point follow each irradiance step, the controller is able always to restore the extracted power in the sub-second timeframes. The steady state ripple is also small, which means that the tracking is accelerated but without causing a large level of oscillations. These results prove the ability of the controller to respond to fast-changing environmental disturbances and retain stable performance.

Case C6: Temperature-dependent results depict the flexibility of the controller to MPP changes in the voltage axis. As would be expected, the optimal PV voltage and power output decreases with rise in temperature. The MPPT scheme is able to overcome this shift and reach the new operating point within the reported tracking range and maintain a low ripple level. This action highlights the fact that response of the controller is not predetermined to the operating assumptions but to the real MPP displacement which is a precondition of outdoor PV usage.

The data reflects the effect of the MPPT perturbation step size (C7 - C9). The larger the step, the more rapid the tracking but the higher the power ripple, and the smaller the step, the less steady the oscillations at the steady-state. The nominal step size provides an equal trade-off between these extremes. Clearly, explicit quantification of both tracking time and ripple per case show that MPPT tuning has a direct impact on dynamic performance; therefore, a careful selection of step size should consider both convergence velocity and steady-state stability.

In stand-alone load disturbance (Cases C10 and C11) the sudden changes in load cause real-time perturbations in PV voltage, power and duty cycle. An increase in load brings about a temporary shortage in power, whilst a reduction in load brings about a short-lived power spike. Under either of the two conditions, the MPPT controller quickly returns to MPP operation within the tracking times recorded in Table 4, and the ripple levels are similar to those found during environmental disturbances. This proves the fact that MPPT stability is not affected by variations in the load.

The behavior is consolidated in the overall system performance (Case C12). The mean tracking time and steady-state ripple is quite close to that of Table 4 and gives a representative idea of long-term MPPT performance. More realistic waveform behavior, such as small-scale oscillations and noise-like behavior, also give testimony to the behavior of controllers as being representative of real operating conditions, and not idealized computer simulation. However, small steady-state oscillations observed in the experimental waveforms are expected due to the perturbation mechanism of the P&O algorithm, converter switching dynamics, and practical sensing noise.

The observed bounded swinging of the waveforms in the experiment can be viewed within the context of the performance trade-offs reported. Under real sensing and switching conditions, in perturb-and-observe schemes of MPPT, such oscillations are a natural outcome of continuous perturbation around the maximum power point. The current implementation still has the limitation of not allowing the amplitude of oscillation to increase, thus suggesting that the selected perturbation step size and filtering policy have reached a compromise between quick convergence and smaller steady-state ripple.

These characteristics of waveforms and performance measures are based on data that has been measured experimentally and then processed in MATLAB in a manner that allows uniform visualization and quantitative comparison without affecting the actual run-time embedded MPPT control execution.

Taken together, the findings indicate that the suggested MPPT method achieves fast dynamic response, limited steady-state oscillations, and strong performance under environmental and load perturbations, which confirm its appropriateness in real PV energy conversion systems.

6. CONCLUSIONS

The dynamics and robustness of a PV maximum power point tracking strategy when it is operated under different environmental conditions, changes in the MPPT tuning parameters, and under stand-alone load disturbances is investigated in this paper. The study was directed at empirically determine the practical MPPT behavior with consistent and dynamic performance metrics and realistic embedded implementation. All results were gathered from hardware measured data, obtained from a NodeMCU ESP8266 based system and analysed and visualised only offline in MATLAB.

The experimental results show the speed of convergence and the stability of steady-state operation for the implemented MPPT strategy in all the scenarios tested. The controller reaches the maximum power point under nominal conditions (1000 W/m², 25 °C) within 0.62 sec, the steady state power ripple is 1.8% and the MPPT efficiency is 98.9%. The tracking time is increased from 0.62 to 0.75 sec (about 21%) or the steady state ripple is increased from 1.8% to 2.1%, as the irradiance is reduced from 1000 to 600 W/m², indicating the sensitivity of the dynamic performance to irradiance variation.

The tracking time, as determined by temperature variation testing, also increases slightly with the PV temperature, to 0.7 sec, a variation of less than 13%, when the PV temperature is increased from 25 °C to 45 °C, while maintaining low steady-state ripple around 2%. This is consistent with a shift in MPP not only in the voltage level but more so in the dynamic tracking behavior, leading to an appreciable degradation.

The effect of MPPT tuning parameters is well understood and can be quantified by using perturbation step-size analysis. The tracking time is improved from 1.05 sec (small step) to 0.48 sec (large step), which represents an improvement rate of about 54%, when the step size of the perturbation is increased. This improvement is however at the expense of increased steady state ripple, from 1.2% up to 3.6%, a nearly 3-fold increase. The results clearly point against the convergence speed versus the steady state stability.

The robustness tests under stand-alone load disturbances show the stability of operation of the MPPT controller under severe load changes. After +50% load, the system restabilizes at MPP within 0.88 sec and after −50% load it takes 0.81 sec for the system to be restabilized at MPP. In both cases the power ripple at steady-state is still below 2.5%, which suggests that there are no significant issues in tracking stability or efficiency when larger load changes occur.

Finally, taking into account all the operating conditions, the MPPT controller has an average tracking time of 0.78 sec, an average steady state ripple of 2.2% and an average MPPT efficiency of 98.1%, which is a good compromise between dynamic response and steady state stability. The findings of these quantitative results prove that it is possible to operate an effective and strong MPPT on a resource-limited embedded system when considering system-level interactions.

This contribution is not in the development of a new MPPT algorithm but in the establishment of an evaluation framework that is both disturbance-aware and experimentally based and explicitly quantifies the effect of the environment, the controller tuning parameters and load disturbances on the dynamic MPPT performance. The proposed framework is directly applicable to stand-alone, smart photovoltaic systems, where rapid convergence, bounded oscillations and reliable operation is crucial.

The present study is based on a classical perturb and observe algorithm for simplicity and reproducibility, but the proposed evaluation framework is algorithm independent and can be directly used for comparison of intelligent and hybrid MPPT strategies in the future study.

While all these contributions have been made, the scope of this work is restricted to the experimentation in controlled conditions and the obtained results are reliable and repeatable, thus offering insights into dynamic and steady state behavior of the MPPT system. Future research will be directed towards adaptive MPPT parameter tuning and further system improvement by implementing advanced data analysis with the current IoT monitoring infrastructure to make the system more robust and intelligent.

REFERENCES

1. K. T. Alao, S. I. U. H. Gilani, K. Sopian, T. O. Alao, and Z. Aslam, "A comprehensive review of radiative cooling technologies and their integration with Photovoltaic (PV) systems: Challenges, opportunities, and future directions," Solar Energy, vol. 292, p. 113445, 2025.
2. L. M. Al-Hilfi, S. Morris, S. H. Y. Ze, B. Venkatesh, C. K. Wai, C. K. Huat, et al., "Comparative simulation of gravity and battery energy storage for solar PV systems: Performance and sustainability insights," Electric Power Systems Research, vol. 256, p. 112864, 2026.
3. D. Afonso, O. Mesbahi, A. Bouich, and M. Tlemçani, "Influence of long-term and short-term solar radiation and temperature exposure on the material properties and performance of photovoltaic panels: A comprehensive review," Energies, vol. 18, p. 5072, 2025.
4. H. Karimi, A. Siadatan, and A. Rezaei-Zare, "A hybrid P&o-fuzzy-based maximum power point tracking (MPPT) algorithm for photovoltaic systems under partial shading conditions," IEEE Access, 2025.
5. P. Priya and A. A. Stonier, "Advancements in maximum power point tracking (MPPT) techniques for solar photovoltaic (PV) applications: A comprehensive review," Energy Conversion and Management: X, p. 101438, 2025.
6. K. Chnini, M. Abdou Tankari, H. Jouini, H. Allagui, M. A. Ibrahim, and E. Touti, "Embedded processor-in-the-loop implementation of ANFIS-based nonlinear MPPT strategies for photovoltaic systems," Energies, vol. 18, p. 2470, 2025.
7. A. Rashid, "A Comprehensive Study on the Effectiveness of Perturb and Observe and Incremental Conductance MPPT Algorithms for Photovoltaic Systems in Dynamic Environments," in 2025 International Conference on Green Energy, Computing and Sustainable Technology (GECOST), 2025, pp. 1-5.
8. R. T. Medikonda and L. Guo, "Performance Evaluation of Artificial Neural Network, Perturb and Observe, and Incremental Conductance MPPT Controllers for Wind Energy Conversion Systems," Electronics, vol. 15, p. 853, 2026.
9. S. Nandi, S. Barnwal, Y. V. Choudhary, T. Goswami, S. Karmakar, S. K. Kundu, et al., "Comparative Evaluation of Classical Perturb and Observe and Incremental Conductance MPPT Algorithms for Photovoltaic Systems," in 2026 9th International Conference on Electronics, Materials Engineering & Nano-Technology (IEMENTech), 2026, pp. 1-6.
10. T. Samavat, M. Nazari, L. Fuhong, and L. Yang, "Optimizing stand-alone PV systems: A metaheuristic-enhanced fuzzy approach for adaptive

MPPT," China Communications, vol. 22, pp. 61-74, 2025.

11. C. M. Nkinyam, C. O. Ujah, C. O. Asadu, B. Anyaka, and P. A. Olubambi, "Development of a low-cost monitoring device for solar electric (PV) system using internet of things (IoT)," Results in engineering, p. 107324, 2025.
12. N. Rouibah, A. Elhammoumi, A. Bouttout, S. Haddad, S. Oukaci, A. Limam, et al., "Smart monitoring of photovoltaic energy systems: An IoT-based prototype approach," Scientific African, p. e02973, 2025.
13. N. Ananthasaravanan and V. Megala, "IoT-Based Hybrid Power System with an AI-Driven MPPT Controller for Z-Source Boost Converters," Iranian Journal of Science and Technology, Transactions of Electrical Engineering, pp. 1-21, 2025.
14. P. J. Hueros-Barrios, F. J. Rodríguez Sánchez, P. Martín Sánchez, C. Santos-Pérez, A. Sangwongwanich, M. Novak, et al., "Digital twin approach for fault diagnosis in photovoltaic plant DC–DC converters," Sensors, vol. 25, p. 4323, 2025.
15. R. Pandey and N. Kumar, "State-Space Based Digital Twin of Single-Stage PV Inverter With Predictive Control for Real-Time Stability Monitoring," IEEE Transactions on Industrial Electronics, 2026.
16. A. Chellakhi and S. El Beid, "High-efficiency MPPT strategy for PV Systems: Ripple-free precision with comprehensive simulation and experimental validation," Results in Engineering, vol. 24, p. 103230, 2024.
17. K. Ullah, M. Ishaq, F. Tchier, H. Ahmad, and Z. Ahmad, "Fuzzy-based maximum power point tracking (MPPT) control system for photovoltaic power generation system," Results in Engineering, vol. 20, p. 101466, 2023.
18. M. M. Gulzar, "Maximum power point tracking of a grid connected PV based fuel cell system using optimal control technique," Sustainability, vol. 15, p. 3980, 2023.
19. A. del Rio, O. Barambones, J. Uralde, E. Artetxe, and I. Calvo, "Particle swarm optimization-based control for maximum power point tracking implemented in a real time photovoltaic system," Information, vol. 14, p. 556, 2023.
20. M. Nivedha and S. Titus, "IoT-based monitoring of smart grid using high-gain converter with optimized maximum power point tracking," Electrical Engineering, vol. 106, pp. 2297-2311, 2024.
21. A.-W. Ibrahim, Z. Fang, R. Li, W. Zhang, J. Xu, V. Zahir, et al., "Intelligent nonlinear PID-Controller combined with optimization algorithm for effective global maximum power point tracking of PV systems," IEEE Access, 2024.
22. A. Boussafa, R. Rabeh, M. Ferfra, and K. Chennoufi, "Experimental test of optimizing maximum power point tracking performance in solar photovoltaic arrays based on backstepping control and optimized by genetic algorithm," Results in Engineering, vol. 23, p. 102746, 2024.
23. A. Elsafi, A. A. Almohammedi, M. Balfaqih, Z. Balfagih, and S. Sabri, "Comparative analysis of maximum power point tracking methods for power optimization in grid tied photovoltaic solar systems," Discover Applied Sciences, vol. 7, p. 976, 2025.
24. Y. Turkay and A. G. Yüksek, "Investigating The Potential of An ANFIS Based Maximum Power Point Tracking Controller for
25. M. A. Azad, A. Sarwar, M. Tariq, F. I. Bakhsh, S. Ahmad, A. S. N. Mohamed, et al., "Global maximum power point tracking for photovoltaic systems under partial and complex shading conditions using a PID based search algorithm (PSA)," IET Renewable Power Generation, vol. 19, p. e70005, 2025.
26. A. K. Abdulrazzaq, G. Bognár, and B. Plesz, "Enhanced single-diode model parameter extraction method for photovoltaic cells and modules based on integrating genetic algorithm, particle swarm optimization, and comparative objective functions," Journal of Computational Electronics, vol. 24, p. 44, 2025.
27. A. Altan, C. Yanarateş, and M. S. Alzaidi, "Enhanced Sensorless Current Control in Boost Converters for EV Fast Charging: Equilibrium Optimization–Tuned Cascaded ANN–Fuzzy Logic Control," IEEE Access, 2026.
28. M. H. Ibrahim, S. P. Ang, M. N. Dani, M. I. Rahman, R. Petra, and S. M. Sulthan, "Optimizing step-size of perturb & observe and incremental conductance MPPT techniques using PSO for grid-tied PV system," IEEE access, vol. 11, pp. 13079-13090, 2023.
29. M. Ismail, M. I. Marei, and M. Mokhtar, "Adaptive Hybrid MPPT for Photovoltaic Systems: Performance Enhancement Under Dynamic Conditions," Sustainability, vol. 18, p. 80, 2025.
30. V. Sukanya, G. Sumesh, S. L. Prakash, and B. Bijukumar, "Analysis of Inductor Current Ripple Minimization in PV-Fed Modular Multilevel DC–DC Converter With Distributed MPPT Control," IEEE Transactions on Circuits and Systems I: Regular Papers, 2025.